Spin-Canting-Induced Band Reconstruction in the Dirac Material $Ca_{1-x}Na_xMnBi_2$

R. Yang,[1] M. Corasaniti,[1] C. C. Le,[2] Z. Y. Liao,[3,4] A. F. Wang,[5,*] Q. Du,[5,6] C. Petrovic,[5,6] X. G. Qiu,[3,4,7] J. P. Hu,[3,8,9] and L. Degiorgi[1]

[1]*Laboratorium für Festkörperphysik, ETH—Zürich, 8093 Zürich, Switzerland*
[2]*Max Planck Institute for Chemical Physics of Solids, Dresden 01187, Germany*
[3]*Beijing National Laboratory for Condensed Matter Physics, Institute of Physics, Chinese Academy of Sciences, Beijing 100190, China*
[4]*School of Physical Sciences, University of Chinese Academy of Sciences, Beijing 100049, China*
[5]*Condensed Matter Physics and Materials Science Department, Brookhaven National Laboratory, Upton, New York 11973, USA*
[6]*Department of Materials Science and Chemical Engineering, Stony Brook University, Stony Brook, New York 11790, USA*
[7]*Songshan Lake Materials Laboratory, Dongguan, Guangdong 523808, China*
[8]*Kavli Institute for Theoretical Sciences and CAS Center for Excellence in Topological Quantum Computation, University of Chinese Academy of Sciences, Beijing 100190, China*
[9]*South Bay Interdisciplinary Science Center, Dongguan, Guangdong Province 523808, China*

(Received 12 November 2019; revised manuscript received 12 February 2020; accepted 6 March 2020; published 30 March 2020)

The ternary $AMnBi_2$ (A is alkaline as well as rare-earth atom) materials provide an arena for investigating the interplay between low-dimensional magnetism of the antiferromagnetic MnBi layers and the electronic states in the intercalated Bi layers, which harbor relativistic fermions. Here, we report on a comprehensive study of the optical properties and magnetic torque response of $Ca_{1-x}Na_xMnBi_2$. Our findings give evidence for a spin canting occurring at $T_s \sim 50$–100 K. With the support of first-principles calculations we establish a direct link between the spin canting and the reconstruction of the electronic band structure, having immediate implications for the spectral weight reshuffling in the optical response, signaling a partial gapping of the Fermi surface, and the dc transport properties below T_s.

DOI: 10.1103/PhysRevLett.124.137201

Even though topological materials, based on novel Dirac-Weyl quasiparticles as well as Majorana fermions [1–6] are fairly well understood, there is still an ongoing effort to understand related elusive quantum phenomena and their potential applications when band topology conspires and coexists with magnetic order, as suggested by the significant anomalous Hall effect and chiral anomalies in Mn_3Sn [7,8] and GdPtBi [9,10].

Recently, the ternary materials $AMnBi_2$ (A is alkaline as well as rare-earth atom) [11,12] have attracted special attention as magnetic topological systems because of the antiferromagnetic (AFM) ground state [Fig. 1(a)] [13] in the presence of anisotropic Dirac cones [14,15], the latter being of relevance for novel electronic devices. The transition Néel temperature (T_N) ranges between 270 and 290 K, with spins along the easy c axis [16,17].

As recognized early in $EuMnBi_2$ [38], it has been conjectured that the interlayer magnetic coupling along the c axis between the Bi square net and AFM order within the MnBi layers parallel to the ab plane plays a central role and may be even the origin of the bumplike feature in the dc resistivity $\rho(T)$, observed in $CaMnBi_2$ at $T_s \sim 50$ K [11,12,39]. By substituting Ca with Na, T_s shifts to higher temperatures and the anomaly of $\rho(T)$ is enhanced [Fig. S1(a) in the Supplemental Material [19]]. The underlying mechanism for this anomaly and whether it reveals an interaction between magnetism and Dirac fermions remains nonetheless to be explored in detail. While both Ca^{2+} and Na^+ are nonmagnetic, the transition at T_s could be the consequence of a spin reorientation, for instance, due to spin canting or weak ferromagnetic order [11,14,39].

In our first attempt [18] to establish a link between the anomaly in $\rho(T)$ and the electronic properties of the title compound, we uncover optical signatures for a partial gapping of the Fermi surface (FS), for energy scales up to 0.2 eV and with onset at T_s. This may reveal the inclination toward a FS instability in topological materials, accompanied by a sizable depletion of the density of states (DOS) at the Fermi level (E_F). The present work intends to precisely address the microscopic origin of the FS gapping. To this goal, we study $Ca_{1-x}Na_xMnBi_2$ at three dopings ($x = 0$, 0.03, and 0.05) and as a function of temperature (T) with magnetic torque measurements, as well as with the support of first-principles calculations. We provide evidence for a spin canting occurring at T_s and leading to a remarkable reconstruction of the electronic band structure, with implications on the reshuffling of spectral weight between the intra- and interband optical response across T_s, and possibly anticipating the generation of Weyl states.

In order to set the stage for the present work, we first revisit our previous optical results [18]. We focus our attention on the real part $\sigma_1(\omega)$ of the in-plane optical

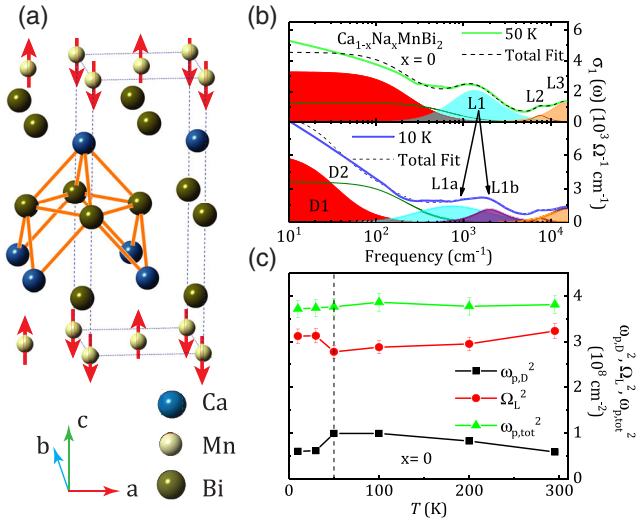

FIG. 1. (a) Crystal structure and C-type AFM order of $Ca_{1-x}Na_xMnBi_2$ (adapted from Ref. [13]). (b) Drude-Lorentz fit and its components of $\sigma_1(\omega)$ for $CaMnBi_2$ at $T \gtrsim T_s$. Experimental data are partially reproduced from Ref. [18]. The fit consists of two Drude terms ($D1$ and $D2$) and three additional Lorentz harmonic oscillators (HOs) ($L1$, $L2$, and $L3$) [19]. Black arrows denote the split of the MIR peak (HO $L1$ above T_s) into two HOs $L1a$ and $L1b$ below T_s (see text). (c) Spectral weight of the Drude components ($\omega_{p,D}^2 = \omega_{p,D1}^2 + \omega_{p,D2}^2$), of the MIR Lorentz HO ($\Omega_L^2 = \Omega_{L1}^2$ above T_s and $\Omega_L^2 = \Omega_{L1a}^2 + \Omega_{L1b}^2$ below T_s) and of their sum ($\omega_{p,\mathrm{tot}}^2 = \omega_{p,D}^2 + \Omega_L^2$), calculated from the fitted strength or plasma frequencies [19].

conductivity for the pristine composition ($x = 0$), shown in Fig. 1(b) from 10 to 4000 cm^{-1} at $50(>T_s)$ and $10(<T_s)$ K. A full review of our original optical findings is provided in Ref. [19], which also details their generality for all Na doping. The narrowing with decreasing T of the low-frequency free-carrier response obviously reflects a better coherence with less scattering from thermal fluctuations. Its high-frequency tail then merges into a series of absorptions. The dominant feature, emphasized here, is the midinfrared (MIR) peak at $\sim$1200 cm^{-1}. We highlight the additional split into two features of this MIR absorption below T_s, which is particularly evident at large Na doping [Figs. S4(a), S4(b), and S5 in Ref. [19]] and bears testimony to a remarkable band reconstruction in coincidence with the spin reorientation at T_s.

With the goal to quantitatively describe the electrodynamic response, we expand our previous discussion of the optical data with their fit within the common Drude-Lorentz phenomenological approach [40]. The resulting fits of $\sigma_1(\omega)$ with their constituent components are displayed in Fig. 1(b). We refer to Ref. [19] for details of the fit procedure and parameters. Complementary to our previous analysis of the integrated spectral weight (SW) [18], we can address here the phenomenological SW, defined as squared plasma frequency ($\omega_{p,Di}^2$) or oscillator strength (Ω_j^2). This allows us to focus the attention on its reshuffling within selected spectral ranges (i.e., related to each fit component). Figure 1(c) shows the T dependence of the Drude ($\omega_{p,D}^2$) and MIR (Ω_L^2) SW as well as of the total one ($\omega_{p,\mathrm{tot}}^2 = \omega_{p,D}^2 + \Omega_L^2$). Since the Lorentz harmonic oscillators (HOs) above 4000 cm^{-1} do not show any noteworthy T dependence (Fig. S7 in Ref. [19]), the conservation of SW only requires that $\omega_{p,\mathrm{tot}}^2$ remains constant. This is indeed the case in Fig. 1(c), and it phenomenologically emphasizes that the reshuffling of SW upon lowering T must essentially occur in the energy interval of about 0.2 eV from E_F between the Drude and MIR contributions in $\sigma_1(\omega)$, suggesting a sizable T dependence of the electronic band structure also at energy scales relevant for transport [18]. Above T_s, the SW of the Drude components increases, while there is a slight suppression of SW in the MIR absorption upon cooling. Since the scattering rates of the Drude components (Fig. S6 in Ref. [19]) do not show any remarkable T dependence above T_s, the decreasing resistivity [Fig. S1(a) in Ref. [19]] is mainly due to the increasing Drude weight. The reinforcement of the Drude weight at the cost of the MIR interband transitions may be the consequence of a reduced Pauli blocking effect upon lowering the chemical potential with decreasing T within the lower Dirac cone [41]. When $T < T_s$, the SW of the Drude contribution is partially suppressed, while the SW of the MIR harmonic oscillator increases, in broad agreement with our conclusions drawn from the integrated SW [18]. The depletion of the intraband SW signifies at least a depletion of DOS at E_F below T_s [18], which is also in line with the suppressed thermal conductivity and Hall carrier density observed earlier [19,39]. In principle, such a reduction of DOS at E_F should result in an increase of $\rho(T)$. However, the scattering rate ($1/\tau$) of the residual Drude components appreciably decreases at low T (Fig. S6 in Ref. [19]), so that the competition between $1/\tau$ and DOS leads to a bumplike feature in $\rho(T)$, as observed in Fig. S1(a) in Ref. [19].

In Ref. [18], we advance the scenario that the experimental signatures in $\sigma_1(\omega)$ and $\rho(T)$ of the transition at T_s are reminiscent of the consequences due to the FS instability, induced by a charge or spin density-wave transition [42]. However, the absence of a jump in the specific heat [Ref. [11] and Fig. S1(b) in Ref. [19]], the smooth behavior of the lattice parameter detected by neutron scattering [16], and the absence of any obvious band folding in angle-resolved photoemission spectroscopy (ARPES) data [15] tend to a scenario for which the reduction of DOS at E_F [i.e., reduction of the Drude SW below T_s, Fig. 1(c)] is due to a reconstruction of the electronic band structure driven by the spin reorientation itself [43], rather than a density-wave order.

Instrumental in solving this dichotomy is then the magnetic torque ($\tau = \mu_0 \mathbf{M} \times \mathbf{H}$, Ref. [19]) experiment. Because of the resolution limit of our commercial instrument at low magnetic fields, we measure the angle dependence of $\tau(\theta)$ at a relatively high field [19]. We show it below (30 K) and above (100 K) T_s in Figs. 2(a)

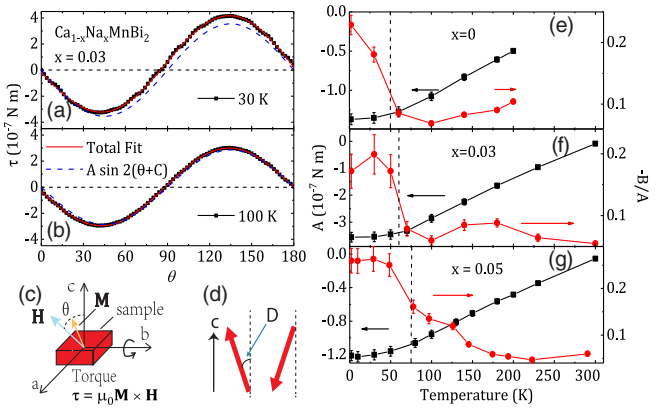

FIG. 2. (a).(b) Magnetic torque ($\tau = \mu_0 \mathbf{M} \times \mathbf{H}$) as a function of the polar angle (θ) of $x = 0.03$ above and below $T_s \sim 60$ K, respectively. Red curve is the total fit after Eq. (1). We refer to Fig. S8 in Ref. [19] for the comprehensive display of the original data at all Na doping. (c),(d) Schematic representations of the experimental configuration for the magnetic torque measurements and the proposed spin canting. The phase shift D is the canting angle. (e)–(g) T dependence of the coefficients A (black) and $-B/A$ (red) of Eq. (1) for $x = 0$, 0.03 and 0.05. The vertical dashed lines mark T_s.

and 2(b), respectively, for $x = 0.03$ as a function of the angle θ between the c axis and applied field of 3 T [Fig. 2(c)]. All curves show roughly a $-\sin 2\theta$ behavior. However, at $T < T_s$ the discrepancy from the $-\sin 2\theta$ functional is more prominent [Fig. 2(a) herein and Fig. S8 in Ref. [19]].

In order to precisely analyze the $\tau(\theta)$ data, we make use of the phenomenological two components fit given by

$$\tau(\theta) = A \sin 2(\theta + C) + B \sin(\theta + D), \qquad (1)$$

where the first term refers to the AFM response and the second one stands for the FM contribution, while C and D are the corresponding phase shifts [19,44–47]. The coefficient A is equal to $\frac{1}{2}\mu_0(\chi_\parallel - \chi_\perp)H^2$ [48]. Since the magnetic moments in $Ca_{1-x}Na_xMnBi_2$ are preferentially aligned along the easy c axis [Fig. 1(a)] of the AFM state [16], one can set $\chi_\parallel = \chi_c$ and $\chi_\perp = \chi_a$; χ_c and χ_a are the magnetic susceptibility along the c and a axis, respectively. The deviation below T_s from the purely AFM response [dashed line in Figs. 2(a) and 2(b)] may be accounted for by the second term in Eq. (1), for which $B = \mu_0 M_s H$, where M_s is the saturated magnetization of the FM response [19,46]. In Fig. S8 of Ref. [19], the $\tau(\theta)$ data are decomposed after the AFM and FM components. Figures 2(e)–2(g) show the T dependence of the resulting A and $-B/A$ coefficients for all investigated compositions. We choose to show $-B/A$ in order to enhance the (weak) FM contribution over the dominating AFM one. Upon cooling, A is negative and its absolute value progressively increases. The T dependence of A is overall consistent with the magnetic susceptibility of $CaMnBi_2$, for which the in-plane one (χ_a) is almost unchanged, and the out-of-plane one along the easy axis (χ_c) decreases continuously with lowering T, both being largely shaped by the AFM state [11]. On the contrary, B, being positive and much smaller than $|A|$, moderately increases from 300 K to T_s, which is associated with a weak FM signature, possibly caused by vacancies [19,43]. Around T_s its enhancement occurs more rapidly, which signifies a net, additional FM response causing the weak bumplike anomaly in χ_c below T_s [11]. The phase shifts C and D are estimated by fit to be 0 and $-10.5 \pm 2°$, respectively [19]. If the FM response is exclusively along the c axis, the phase shift D should be zero. Therefore, the finite D value signals the presence of a tilting of about 10° of the magnetic moments from the c axis, as shown in Fig. 2(d), which is particularly relevant below T_s [Fig. S8(d) in Ref. [19]] and gives rise to a canted AFM order. The presence of in-place projected magnetic moments below T_s is also supported by our data collected at fixed angles upon sweeping the magnetic field (Fig. S9 in Ref. [19]). It is fair noting that, besides the already mentioned tiny discrepancies from stoichiometry, the spin flop [49] could also lead to a net FM response. Nonetheless, its absence in the title compound [12], the phase shift $D \neq 0$ itself, and the encountered FM behavior in both the in-plane and out-of-plane susceptibility (Fig. S2 in Ref. [19]) further favor the spin-canting scenario, a signature of growing importance in topological magnetic materials [43,50].

We introduce here the calculation of the electronic band structure of $CaMnBi_2$ based on the density functional theory, which is of paramount importance toward a comprehensive account of the experimental findings deployed so far. Figure 3(a) displays the band structure in the C-type AFM state [Fig. 1(a)] without canting, while Fig. 3(b) shows it with 10° canting angle. Upon switching on the spin canting, the exchange effect caused by the net FM response leads to a split of almost all bands into spin-up and spin-down dominated branches [Fig. 3(b)]. However, near E_F only the holelike bands from the intercalated Bi p_z orbital (which predominantly hybridizes with the Mn $d_{x^2-y^2}$ orbital through the intralayer Bi p_z orbital, Fig. S10 in Ref. [19]) are remarkably split, while the linear bands from the intercalated Bi $p_{x/y}$ orbitals are almost unchanged [19]. This means that the $p_{x/y}$ orbitals are marginal to the magnetism in MnBi layers and less sensitive to the net FM order. The consequences of canting are also imaged by the changes of DOS at E_F, shown in Figs. 3(c)–3(e). We observe an overall depletion of DOS at E_F, which mainly affects the p_z orbital contribution [Fig. 3(d)], while negligible variations are encountered at E_F for $p_{x/y}$ orbitals [Fig. 3(e)].

Supported by our first-principles calculations, we propose to interpret the MIR absorption in $\sigma_1(\omega)$ above T_s [Fig. 1(b) herein and Figs. S4(a) and S4(b) in Ref. [19]] in

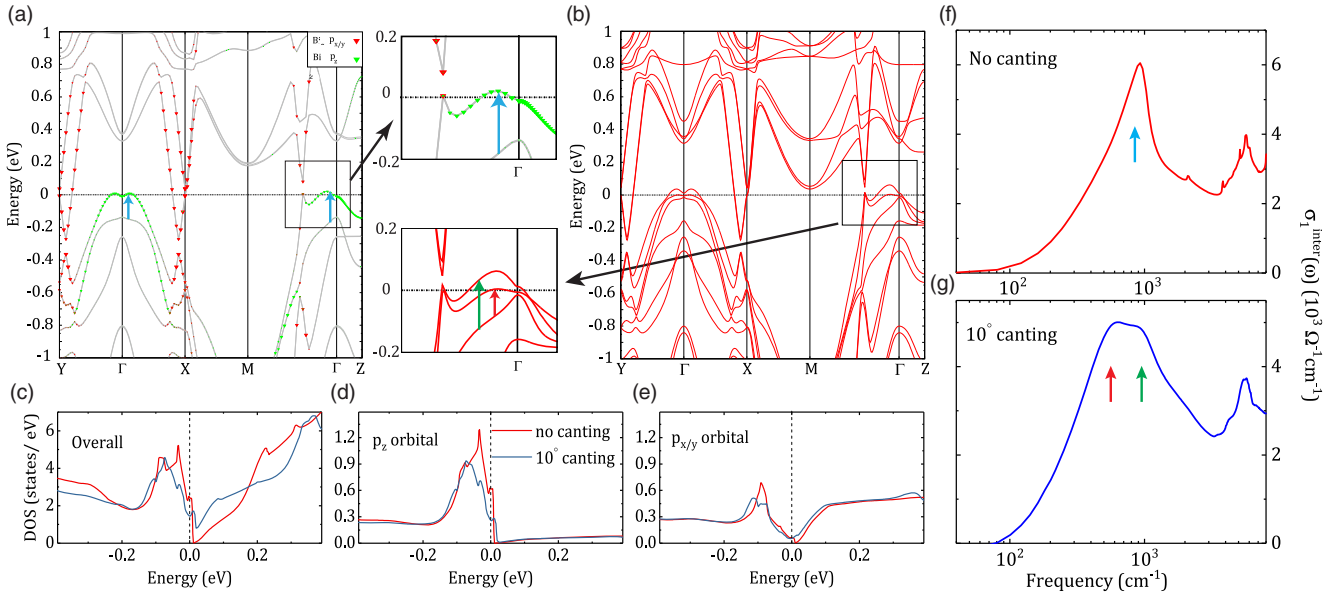

FIG. 3. (a),(b) Electronic band structure without (a) and with (b) spin canting. In (a), the contribution from different Bi p orbitals in the square net are denoted by different colors [19]. Insets: Enlargement of the electronic band structure inside the black boxes of the main panels (a) and (b). (c)–(e) Total density of states (DOS) (c) as well as partial one for p_z (d) and $p_{x/y}$ (e) orbitals. (f),(g) Calculated interband contribution [$\sigma_1^{\text{inter}}(\omega)$] of the optical conductivity [19] from the band structure without (f) and with (g) spin canting. The arrows in (a),(b) and (f),(g) (blue without, and red and green after canting) highlight the interband transitions responsible for the MIR absorption and its split in $\sigma_1(\omega)$ [Fig. 1(b) herein and Figs. S4(a) and S4(b) in Ref. [19]].

terms of the interband transition between the Mn $d_{x^2-y^2}$-dominated band and the intercalated Bi p_z-dominated hole pocket around the Γ point of the Brillouin zone (BZ), as indicated by the blue arrows in Fig. 3(a) and its inset. Indeed, the calculated (interband) optical conductivity $\sigma_1^{\text{inter}}(\omega)$ shows an excitation at a similar energy scale [Fig. 3(f)]. This absorption reflects the $p-d$ hybridization between Mn and intercalated Bi orbitals, which are involved in the interlayer magnetic coupling. On the other hand, the spin-canting-induced split of the intercalated Bi p_z orbital around the Γ point of the BZ [insets of Fig. 3(b)] leads to a shift above E_F of one branch and thus induces a hole pocket (i.e., empty states). The resulting enhanced hole character also generates the possibility for additional interband transitions [Fig. 3(b) and its inset]. Concomitantly, the MIR feature in $\sigma_1^{\text{inter}}(\omega)$ splits into two peaks [indicated by the red and green arrows in Figs. 3(b) and 3(g)], in excellent agreement with the experimental findings [Fig. 1(b) herein and Fig. S4 in Ref. [19]]. Moreover, the related reduction of DOS at E_F with spin canting [Figs. 3(c)–3(e)] foresees the depletion of the Drude-like SW in $\sigma_1(\omega)$ [Fig. 1(c) and Refs. [18,19]].

So far, we have focused the attention on the impact of the experimentally determined spin canting on the electronic band structure. The outcome of our first-principles calculations similarly catches a glimpse of the driving mechanism leading to the spin canting itself. We propose that it resides in the interlayer magnetic coupling between the Mn d orbitals, mediated by the p orbitals of the intercalated Bi square nets [Fig. 1(a)]. Such a scenario encounters the basic features of the superexchange magnetic coupling (details in Ref. [19]) and may reveal the microscopic origin of the anomaly in $\rho(T)$ and its Na doping dependence. Indeed, with Na doping, the reduced interlayer distance enhances the overlap between the Bi p and Mn d orbitals and thus the $p-d$ hopping integral, while more unoccupied states as a consequence of the hole doping in the Bi p_z orbital should equally reduce the energy difference between the relevant occupied p/d orbitals. All this leads to an enhancement of the interlayer magnetic coupling, which favors a higher transition temperature T_s in accord with $\rho(T)$ of $Ca_{1-x}Na_xMnBi_2$ [Fig. S1(a) in Ref. [19]]. Furthermore, we speculate that with a larger hole pocket, as for Na-doped $CaMnBi_2$ because of the robust downward energy shift of the chemical potential, even more DOS at E_F will be consumed by spin canting (also irrespective of correlation effects, Fig. S11 in Ref. [19]). Thus, a more obvious anomaly may be foreseen in $\rho(T)$, in trend with the experimental observations [Fig. S1(a) in Ref. [19]] despite the impact of the decreasing scattering rate at $T < T_s$ (Fig. S6 in Ref. [19]).

Finally, we shall compare the title compound with the structurally similar $YbMnBi_2$. Even though they both share the same fingerprints in their electronic band structure, one can notice that in $YbMnBi_2$ all bands around the Γ point are below E_F [50,51], while those in $CaMnBi_2$ cross E_F. The hopping between the $p-d$ orbitals, introduced above for mediating the magnetic interlayer coupling, is then blocked

in $YbMnBi_2$, making the electronic environment for spin canting less favorable. Moreover, neutron scattering investigations [16,52] determine a smaller single-ion anisotropy in $CaMnBi_2$ than in $YbMnBi_2$. The smaller the latter parameter, the weaker the spins will be constrained along the easy c axis, so that the spin canting takes place more easily in $CaMnBi_2$.

ARPES investigations on $YbMnBi_2$ [50], though, give evidence for the realization of a type-II Weyl semimetal and it was claimed that the necessary breaking of the time-reversal symmetry (TRS) is driven by spin canting, as well. This is however debated and experimentally controversial. Recent neutron scattering measurements on $YbMnBi_2$ [52] do not detect any fingerprints of spin canting in the bulk but cannot exclude that it might happen at the sample surface only (where ARPES is sensitive), for instance, as a consequence of Yb vacancies. This possibility could reconcile such a variety of yet contrasting data [51].

Obviously, if spin canting is the principle driving mechanism for the reconstruction of the electronic band structure below T_s, as revealed by our experiments, we might expect the realization of Weyl states in Na-doped $CaMnBi_2$ as a consequence of the broken TRS. This is of wider interest because of the peculiar Dirac band crossing along a continuous line in momentum space in $CaMnBi_2$ [53]. There is thus a pressing need for high-resolution ARPES experiments at $T < T_s$ in $Ca_{1-x}Na_xMnBi_2$, paired with neutron scattering investigations on their single crystals.

The authors thank A. Boothroyd for fruitful discussions. This work was partially supported by the Swiss National Science Foundation (SNSF). Work at Brookhaven National Laboratories was supported by the U.S. DOE-BES, Division of Materials Science and Engineering, under Contract No. DE-SC0012704. X. G. Q. acknowledges the support from the National Science Foundation of China (Projects No. 11974412 and No. 11774400) and MOST (Project No. 2017YFA0302903). J. P. H. is supported by the Ministry of Science and Technology of China 973 program (Grant No. 2017YFA0303100), NSFC (Grant No. NSFC-11888101), and the Strategic Priority Research Program of CAS (Grant No. XDB28000000).

*Present address: School of Physics, Chongqing University, Chongqing 400044, China.

[1] M. Z. Hasan and C. L. Kane, Rev. Mod. Phys. **82**, 3045 (2010).
[2] K. S. Novoselov, A. K. Geim, S. V. Morozov, D. Jiang, M. I. Katsnelson, I. V. Grigorieva, S. V. Dubonos, and A. A. Firsov, Nature (London) **438**, 197 (2005).
[3] C.-Z. Chang *et al.*, Science **340**, 167 (2013).
[4] J. Li, Y. Li, S. Du, Z. Wang, B.-L. Gu, S.-C. Zhang, K. He, W. Duan, and Y. Xu, Sci. Adv. **5**, eaaw5685 (2019).
[5] X.-L. Qi and S.-C. Zhang, Rev. Mod. Phys. **83**, 1057 (2011).
[6] Q. Wang, Y. Xu, R. Lou, Z. Liu, M. Li, Y. Huang, D. Shen, H. Weng, S. Wang, and H. Lei, Nat. Commun. **9**, 3681 (2018).
[7] A. K. Nayak, J. E. Fischer, Y. Sun, B. Yan, J. Karel, A. C. Komarek, C. Shekhar, N. Kumar, W. Schnelle, J. Kübler, C. Felser, and S. S. P. Parkin, Sci. Adv. **2**, e1501870 (2016).
[8] S. Nakatsuji, N. Kiyohara, and T. Higo, Nature (London) **527**, 212 (2015).
[9] T. Suzuki, R. Chisnell, A. Devarakonda, Y.-T. Liu, W. Feng, D. Xiao, J. W. Lynn, and J. G. Checkelsky, Nat. Phys. **12**, 1119 (2016).
[10] M. Hirschberger, S. Kushwaha, Z. Wang, Q. Gibson, S. Liang, C. A. Belvin, B. A. Bernevig, R. J. Cava, and N. P. Ong, Nat. Mater. **15**, 1161 (2016).
[11] J. B. He, D. M. Wang, and G. F. Chen, Appl. Phys. Lett. **100**, 112405 (2012).
[12] A. Wang, D. Graf, L. Wu, K. Wang, E. Bozin, Y. Zhu, and C. Petrovic, Phys. Rev. B **94**, 125118 (2016).
[13] A. Zhang, C. Liu, C. Yi, G. Zhao, T. L. Xia, J. Ji, Y. Shi, R. Yu, X. Wang, C. Chen, and Q. Zhang, Nat. Commun. **7**, 13833 (2016).
[14] J. Park, G. Lee, F. Wolff-Fabris, Y. Y. Koh, M. J. Eom, Y. K. Kim, M. A. Farhan, Y. J. Jo, C. Kim, J. H. Shim, and J. S. Kim, Phys. Rev. Lett. **107**, 126402 (2011).
[15] Y. Feng, Z. Wang, C. Chen, Y. Shi, Z. Xie, H. Yi, A. Liang, S. He, J. He, Y. Peng, X. Liu, Y. Liu, L. Zhao, G. Liu, X. Dong, J. Zhang, C. Chen, Z. Xu, X. Dai, Z. Fang, and X. J. Zhou, Sci. Rep. **4**, 5385 (2015).
[16] Y. F. Guo, A. J. Princep, X. Zhang, P. Manuel, D. Khalyavin, I. I. Mazin, Y. G. Shi, and A. T. Boothroyd, Phys. Rev. B **90**, 075120 (2014).
[17] M. C. Rahn, A. J. Princep, A. Piovano, J. Kulda, Y. F. Guo, Y. G. Shi, and A. T. Boothroyd, Phys. Rev. B **95**, 134405 (2017).
[18] M. Corasaniti, R. Yang, A. Pal, M. Chinotti, L. Degiorgi, A. Wang, and C. Petrovic, Phys. Rev. B **100**, 041107(R) (2019).
[19] See Supplemental Material at http://link.aps.org/supplemental/10.1103/PhysRevLett.124.137201 for further details of the sample's characterization and experimental techniques as well as for complementary data and analysis, which includes Refs. [20–37].
[20] K. Wang, D. Graf, L. Wang, H. Lei, S. W. Tozer, and C. Petrovic, Phys. Rev. B **85**, 041101(R) (2012).
[21] F. Pfuner, P. Lerch, J.-H. Chu, H.-H. Kuo, I. R. Fisher, and L. Degiorgi, Phys. Rev. B **81**, 195110 (2010).
[22] C. F. Miclea, H. D. Hochheimer, B. Martin, C. Miclea, and T. Ohtani, New J. Phys. **15**, 083008 (2013).
[23] F. Rullier-Albenque, D. Colson, A. Forget, and H. Alloul, Phys. Rev. Lett. **103**, 057001 (2009).
[24] N. P. Ong and P. Monceau, Phys. Rev. B **16**, 3443 (1977).
[25] R. S. Kwok, G. Grüner, and S. E. Brown, Phys. Rev. Lett. **65**, 365 (1990).
[26] D. Starešinić, A. Kiš, K. Biljaković, B. Emerling, J. W. Brill, J. Souletie, H. Berger, and F. Lévy, Eur. Phys. J. B **29**, 71 (2002).
[27] W. Zhang, K. Nadeem, H. Xiao, R. Yang, B. Xu, H. Yang, and X. G. Qiu, Phys. Rev. B **92**, 144416 (2015).
[28] J. Kanamori, in Magnetism, edited by H. Suhl and G. T. Rado (Academic Press, New York, 1973), Vol. **1**, Chap. 4.

[29] G. Kresse and J. Hafner, Phys. Rev. B **47**, 558(R) (1993).
[30] G. Kresse and J. Furthmüller, Comput. Mater. Sci. **6**, 15 (1996).
[31] G. Kresse and J. Furthmüller, Phys. Rev. B **54**, 11169 (1996).
[32] H. J. Monkhorst and J. D. Pack, Phys. Rev. B **13**, 5188 (1976).
[33] P. Blaha, K. Schwarz, P. Sorantin, and S. Trickey, Comput. Phys. Commun. **59**, 399 (1990).
[34] F. J. Ohkawa and N. Matsumoto, J. Phys. Soc. Jpn. **63**, 602 (1994).
[35] F. Ma, W. Ji, J. Hu, Z.-Y. Lu, and T. Xiang, Phys. Rev. Lett. **102**, 177003 (2009).
[36] C.-Y. Moon and H. J. Choi, Phys. Rev. Lett. **104**, 057003 (2010).
[37] Z. Wang, P. Zhang, G. Xu, L. K. Zeng, H. Miao, X. Xu, T. Qian, H. Weng, P. Richard, A. V. Fedorov, H. Ding, X. Dai, and Z. Fang, Phys. Rev. B **92**, 115119 (2015).
[38] A. F. May, M. A. McGuire, and B. C. Sales, Phys. Rev. B **90**, 075109 (2014).
[39] K. Wang, L. Wang, and C. Petrovic, Appl. Phys. Lett. **100**, 112111 (2012).
[40] M. Dressel and G. Grüner, *Electrodynamics of Solids* (Cambridge University Press, Cambridge, England, 2002).
[41] The spin-orbit coupling gaps the Dirac cones and moves the Fermi level into the lower cone [15]. Upon lowering T, the intraband response is thus more favorable than the excitation across the gapped Dirac cones.
[42] G. Grüner, *Density Waves in Solids*, (Perseus Books Group, Reading (MA), 2000).
[43] J. Y. Liu, J. Hu, Q. Zhang, D. Graf, H. B. Cao, S. M. A. Radmanesh, D. J. Adams, Y. L. Zhu, G. F. Cheng, X. Liu, W. A. Phelan, J. Wei, M. Jaime, F. Balakirev, D. A. Tennant, J. F. DiTusa, I. Chiorescu, L. Spinu, and Z. Q. Mao, Nat. Mater. **16**, 905 (2017).
[44] S. Weyeneth, P. J. W. Moll, R. Puzniak, K. Ninios, F. F. Balakirev, R. D. McDonald, H. B. Chan, N. D. Zhigadlo, S. Katrych, Z. Bukowski, J. Karpinski, H. Keller, B. Batlogg, and L. Balicas, Phys. Rev. B **83**, 134503 (2011).
[45] M. D. Watson, A. McCollam, S. F. Blake, D. Vignolles, L. Drigo, I. I. Mazin, D. Guterding, H. O. Jeschke, R. Valentí, N. Ni, R. Cava, and A. I. Coldea, Phys. Rev. B **89**, 205136 (2014).
[46] L. Chen, F. Yu, Z. Xiang, T. Asaba, C. Tinsman, B. Lawson, P. M. Sass, W. Wu, B. L. Kang, X. Chen, and L. Li, Phys. Rev. Applied **9**, 024005 (2018).
[47] H. Xiao, T. Hu, C. C. Almasan, T. A. Sayles, and M. B. Maple, Phys. Rev. B **73**, 184511 (2006).
[48] K. Yosida, Prog. Theor. Phys. **6**, 691 (1951).
[49] H. Masuda, H. Sakai, M. Tokunaga, M. Ochi, H. Takahashi, K. Akiba, A. Miyake, K. Kuroki, Y. Tokura, and S. Ishiwata, Phys. Rev. B **98**, 161108(R) (2018).
[50] S. Borisenko, D. Evtushinsky, Q. Gibson, A. Yaresko, K. Koepernik, T. Kim, M. Ali, J. van den Brink, M. Hoesch, A. Fedorov, E. Haubold, Y. Kushnirenko, I. Soldatov, R. Schäfer, and R. J. Cava, Nat. Commun. **10**, 3424 (2019).
[51] D. Chaudhuri, B. Cheng, A. Yaresko, Q. D. Gibson, R. J. Cava, and N. P. Armitage, Phys. Rev. B **96**, 075151 (2017).
[52] J.-R. Soh, H. Jacobsen, B. Ouladdiaf, A. Ivanov, A. Piovano, T. Tejsner, Z. Feng, H. Wang, H. Su, Y. Guo, Y. Shi, and A. T. Boothroyd, Phys. Rev. B **100**, 144431 (2019).
[53] G. Lee, M. A. Farhan, J. S. Kim, and J. H. Shim, Phys. Rev. B **87**, 245104 (2013).